

---

# COLORA: EFFICIENT FINE-TUNING FOR CONVOLUTIONAL MODELS WITH A STUDY CASE ON OPTICAL COHERENCE TOMOGRAPHY IMAGE CLASSIFICATION

---

Mariano Rivera, Angello Hoyos  
 Centro de Investigacion en Matematicas AC  
 Guanajuato, Gto., 36240, Mexico  
 mrivera@ciimat.mx

## ABSTRACT

We introduce the Convolutional Low-Rank Adaptation (CoLoRA) method, designed explicitly to overcome the inefficiencies found in current CNN fine-tuning methods. CoLoRA can be seen as a natural extension of the convolutional architectures of the Low-Rank Adaptation (LoRA) technique. We demonstrate the capabilities of our method by developing and evaluating models using the widely adopted CNN backbone pre-trained on ImageNet. We observed that this strategy results in a stable and accurate coarse-tuning procedure. Moreover, this strategy is computationally efficient and significantly reduces the number of parameters required for fine-tuning compared to traditional methods. Furthermore, our method substantially improves the speed and stability of training. Our case study focuses on classifying retinal diseases from optical coherence tomography (OCT) images, specifically using the OCTMNIST dataset. Experimental results demonstrate that a CNN backbone fine-tuned with CoLoRA surpasses nearly 1% in accuracy. Such a performance is comparable to the Vision Transformer, State-space discrete, and Kolmogorov-Arnold network models.

**Keywords** Convolutional Networks · Fine-tuning · Transfer Learning · LoRA · OCTMNIST dataset

## 1 Introduction

In recent times, neural network models have increased significantly in complexity and size, particularly evident in foundational large language models (LLMs) [1, 2]. Such models often have parameter counts ranging from tens of billions to trillions; for instance, GPT-4 (Generative Pre-trained Transformer) has approximately 1.5 trillion parameters, LLaMA 3.2 (Large Language Model Meta AI) has 90 billion parameters, and DeepSeek-V3 comprises 671 billion parameters [3]. Consequently, efficiently fine-tuning these large foundational models for specific applications has become essential. Efficient Parameter Fine-Tuning (EPFT) encompasses various algorithms designed to freeze the original backbone while fine-tuning a smaller set of new parameters. EPFT methods have proven effective in tasks involving vision and text [4, 5, 6]. Among EPFT strategies, LoRA (Low-Rank Adaptation) stands out for its effectiveness and simplicity. For medical image analysis, adapters have facilitated the fine-tuning of transformer-based architectures, such as the Segment Anything Model (SAM) [7, 8]. There are a few notable examples; EPFT techniques remain relatively unexplored within the medical imaging domain [9]. The reason may be that Transfer Learning using convolutional neural networks (CNNs) is still one of the most common strategies in medical image analysis [10, 11].

Although CNNs are generally smaller compared to LLMs, effective fine-tuning remains crucial for ensuring optimal performance and efficient deployment in practical scenarios. However, limited attention has been paid to improving the fine-tuning methods specifically tailored for convolutional neural networks (CNNs). In this work, we introduce the Convolutional Low-Rank Adaptation (CoLoRA) layer, designed explicitly to overcome inefficiencies found in current CNN fine-tuning methods. CoLoRA can be seen as a natural extension of the LoRA technique to convolutional architectures. While LoRA updates dense layer weights by factorizing them into two low-rank matrices (see Fig. 1(a)), our method updates convolutional kernels (Fig. 1(b)) by decomposing them into pixel-wise ( $1 \times 1$ ) and depthwise convolutions (with spatial dimensions but only one channel); see Fig. 1(c).

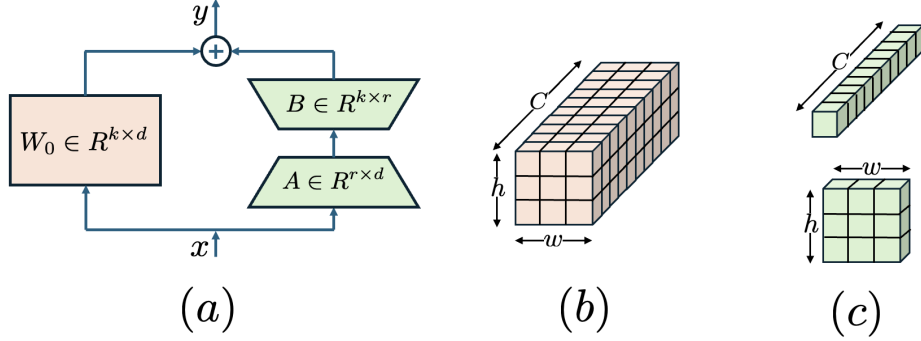


Figure 1: (a) General scheme of LoRA. (b) 2D convolutional kernel (filter). (c) A 2D convolution is separated into two kernels: a depthwise kernel and a pointwise kernel.

To demonstrate the capabilities of CoLoRA, we developed and evaluated models using two widely adopted CNN backbones: VGG16 [12] and ResNet50 [13, 14], both pre-trained on ImageNet. Our case study focuses on classifying retinal diseases from optical coherence tomography (OCT) images, specifically using the OCTMNIST dataset. This dataset categorizes images into four classes: Choroidal Neovascularization (ChN), Diabetic Macular Edema (DME), Drusen, and Normal. We selected this particular problem due to its clinical relevance and because existing results have shown significant variability and dependency on training strategies, primarily due to class imbalance.

Our CoLoRA layer can straightforwardly be generalized for fine-tuning convolutional layers in other dimensions than two; provided that we have a ready implementation of the Depthwise Convolution Layer. The strategy, inspired by InceptionNet [15], is first to look for cross-channel correlations to reduce the dimension of the tensors along the channels. Next, the model looks for spatial correlations in a lower-dimension tensor (a tensor with a single channel). This order of operations is computationally efficient and significantly reduces the number of parameters required for fine-tuning compared to traditional methods. Furthermore, our method substantially improves the speed and stability of training.

Experimental comparison results showing that a CNN-based model using a pre-trained network and fine-tuned with CoLoRA surpasses improves accuracy by close 1% when compared with state-of-the-art methods: Vision Transformers [16, 17], State Spaces Diskretizations [18], and Kolmogorov-Arnold Network [19] Models. Our best-performing model achieving an accuracy of 0.963 and an area under the receiver operating characteristic curve (AUC) of 0.95 match or surpass these state-of-the-art results.

The remainder of this paper is structured as follows. Section 2 reviews related work, Section 3 details the proposed CoLoRA method, Section 4 presents experimental validations and results, and Section 5 offers conclusions and outlines future research directions.

## 2 Related Methods

### 2.1 LoRA: Low-Rank Adaptation

The Low Rank Adaptation (LoRA) method is designed to efficiently fine-tune large pre-trained models for specific tasks [20]. This is achieved by introducing low-rank learnable matrices into the model, allowing most of the original parameters to remain frozen. This significantly reduces the computational and storage costs associated with full fine-tuning while maintaining high task performance.

Given the pre-trained layer that computes  $y = W_0 x$ , then the fine-tuning consists on updating the weight matrix  $W_0 \in \mathbb{R}^{k \times d}$  with  $\Delta W$  such that

$$y = (W_0 + \Delta W) x = W_0 x + \Delta W x; \quad (1)$$

with  $x \in \mathbb{R}^d$  and  $y \in \mathbb{R}^k$ . LoRA constrains the weight updates  $\Delta W$  as a product of two low-rank matrices:

$$\Delta W = B A, \quad (2)$$

where  $A \in \mathbb{R}^{r \times d}$  and  $B \in \mathbb{R}^{k \times r}$ , with  $r \ll \min(d, k)$ . Here,  $d$  and  $k$  are the dimensions of the original weight matrix, and  $r$  is the rank, which is typically set to a small value. In LoRA the fine-tuning is achieved by freezing the pre-trained weights  $W_0$  and training the Low-Rank Matrices  $A$  and  $B$ ; setting initially  $A \sim \mathcal{N}(0, \sigma^2)$  and  $B = 0$ . Figure 1.a illustrates LoRA. The advantages of LoRA are the following.

- **Efficiency:** By keeping most of the original parameters fixed, LoRA requires fewer trainable parameters and reduces memory usage.
- **Modularity:** The low-rank updates can be stored and applied separately, making the method highly modular.
- **Scalability:** LoRA is suitable for fine-tune very large models without retraining or duplicating the entire model.

LoRA is widely used for fine-tuning foundational models in the domains of natural language processing (NLP), computer vision, and other domains where fine-tuning large models is computationally expensive [1, 2, 21]. In particular, in Transformers-based architectures where the attention mechanism is based on dense matrices (in general denoted by  $Q$ ,  $K$ , and  $V$ ) with dimensions  $d = k$  and  $d$  large; e.g.,  $d = 1024$ . Its modular nature also makes it compatible with several architectures and training regimes.

## 2.2 Convolutional Layers

The Convolutional Layer is the fundamental building block of Convolutional Neural Networks (CNNs) designed to process grid-like data such as images [12, 13, 14, 22]. Convolutional layers are used in image classification, object detection, segmentation, and more. They are key to achieving state-of-the-art performance in tasks involving visual data. Performs a convolution operation by applying a set of learnable filters (kernels) to input data, extracting spatial hierarchies of features such as edges, textures, and shapes. For a single input feature map  $I \in \mathbb{R}^{H,W,C}$  and filter  $K \in \mathbb{R}^{h,w,C}$ , the output feature map  $O \in \mathbb{R}^{H,W}$  is computed as:

$$O(x, y) = K \circledast I = \sum_{i,j,k} K(i, j, k) I(x + i, y + j, k) \quad (3)$$

where  $\circledast$  denotes the correlation operation,  $(x, y)$  the spatial position, and  $(i, j, k)$  the indices of the filter. The filters operate on small local regions of the input image, allowing the network to capture spatial relationships. Each filter is applied across the entire input, significantly reducing the number of parameters. Figure 1b depicts a 2D-convolutional filter or kernel with dimension  $(h \times w \times C)$ ; i.e., height, width and Channels. Although, the filter has dimensions, it is applied by shifting the kernel only in the spatial coordinates, meanwhile the kernel depth  $C$  is equal to the number of channels in the input  $I$ . In addition, multiple filters extract different features, allowing rich representations of the data. The most relevant hyper-parameters of the convolutional layers are: the *number of filters* that specify the number of unique features to extract, the *filter size* that determines the receptive field of the filter (e.g.,  $3 \times 3, 5 \times 5$ ), the *stride* that defines the step size of the filter spatial displacement, and the *padding* that defines the added borders to the input to control the spatial dimensions of the output.

## 2.3 Separable Convolutional Layers

Separable convolutions are widely used in modern architectures like Xception [23] and MobileNet [24] to achieve state-of-the-art performance with lower computational demands. They are an efficient variant of standard convolutional layers that decompose the convolution operation into smaller, more computationally efficient steps. Depthwise separable convolutions factorize standard convolutions into two convolutions. First, apply a single filter  $K_d$  per input channel, and second, use a  $1 \times 1$  filter  $K_p$  to combine the outputs of the first convolution. Mathematically, given an input tensor of shape  $(H, W, C)$  and a filter of size  $(h, w, C)$ . The depthwise step applies to each channel a filter of size  $(h, w)$  to produce  $C$  feature maps:

$$Z(x, y, k) = K_d \circledast I = \sum_{i,j,k} K_d(i, j) I(x + i, y + j, k) \quad (4)$$

Then, the pointwise step applies  $D$  (a  $1 \times 1$  filter) to combine the  $C$  feature maps:

$$O(x, y) = K_p \circledast Z = \sum_k K_p(k) Z(x, y, k) \quad (5)$$

Such computations, (4) and (5), can be expressed by

$$O = K_p \circledast K_d \circledast I \quad (6)$$

## 2.4 CNN Adapter

LoRA is a particular case of a general family of adapters introduced in the context of transformers [25, 26]. The adapter was initially proposed by Rebuffi et al. for CNNs [27, 28]. The Rebuffi’s adapter extends the original network with

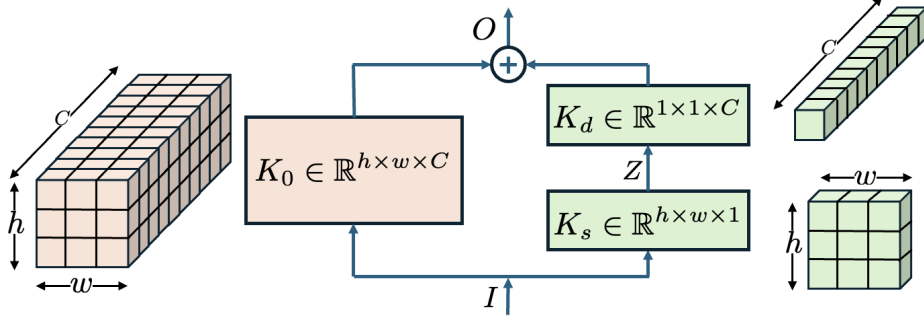


Figure 2: CoLoRA Layer.

parametric residual modules. The strategy is to train the residual module, keeping the original parameters (weights or filters) unchanged. The purpose was to develop a residual network (module) suitable for multiple domains. More recently, the CNN adapter adds to each convolutional block a residual module layer that consists of a convolution, a normalization, and a (GELU) activation [29]; for better performance, such adapters are also combined with an update version of Rebuffi’s adapter: the Housby’s adapters (CHAPTER) [30]. In any case, CNN adapters are designed to adjust CNNs to different domains at the cost of increasing the model complexity.

On the other hand, LoRA took a step further, introducing residual modules (of low rank) that update the original modules with a sum. Hence, such residual modules can be merged into the original model parameter. Therefore, LoRA can preserve the number of parameters in the tuned model. Our work is more in the LoRA spirit: improving the models’ performance while preserving (in inference mode) the model complexity.

### 3 Method

Pre-trained backbones trained on unrelated datasets are employed for developing domain-specific models. The standard training procedure involves two stages. First, the backbone acts as a fixed universal feature extractor, transforming input data into a feature space suitable for training subsequent domain-specific layers. The second stage fine-tunes a subset of weights within the backbone alongside the newly added layers, further improving model accuracy.

#### 3.1 Convolutional Low Rank Adaptation

The CoLoRA is the natural extension of the LoRA paradigm to convolutional networks. While LoRA constrains the update weights (matrix)  $\Delta W$  by the product of two low-rank matrices, CoLoRA approximates the kernel updating  $\Delta K$  by applying separable convolutions. Particularly, CoLoRA constrains the updates to be expressed with a learnable depthwise separable convolution and keeps frozen the pre-trained weights. This significantly reduces the number of learnable parameters, especially when the number of input channels and filters is large. We observed that this strategy results in a stable and accurate fine-tuning procedure.

Given the pre-trained convolutional layer that computes

$$O = K_0 * I, \quad (7)$$

then the CoLoRA fine-tuning consists on updating the kernel  $K_0 \in \mathbb{R}^{h \times w \times C}$  with  $\Delta K$  such that

$$O = (K_0 + \Delta K) \otimes x = W_0 \otimes x + \Delta W \otimes I; \quad (8)$$

where we constraint the kernel update  $\Delta K$  to be a separable kernel:

$$\Delta K = K_p \otimes K_d. \quad (9)$$

The initialization of a CoLoRA layer is carried out as follows. The convolutional layer is initialized with the pre-trained weights. The spatial kernel layer  $K_s$  is created preserving the following properties of the pre-trained convolutional layer: *data type, number of filters, kernel size, stride, padding, data format, dilation rate, activation, use of bias*. The weights are initialized as the pre-trained layer. Finally, the weights of the kernel  $K_d$  are initialized with zeros. Figure 2 presents a scheme of the CoLoRA filter updating process inspired by the LoRA scheme; see Fig. 1a. It is important to note that the bias vector of the convolutional filters can and should also be updated. Until now, we have omitted to

mention them to keep the presentation simple; however, if  $b_0 \in \mathbb{R}^C$  is the pre-trained bias vector, then the update is a vector  $\Delta b$  of the same dimension.

The benefits of using separable convolutions are their **efficiency**, significant reduction in computational complexity and number of parameters; **flexibility**, limited computational resource requirements; and **performance**, competitive accuracy compared to standard convolutions. Our approach also has the advantages of the LoRA update scheme. Similar to LoRA, once we have trained the separable convolution weights  $(K_d, K_p)$ , we update the original weights with

$$K_0 \leftarrow K_0 + K_p \circledast K_d, \quad (10)$$

and the bias with

$$b_0 \leftarrow b_0 + \Delta b. \quad (11)$$

Once kernel  $K_0$  and bias  $b_0$  are updated, the kernels  $(K_d, K_p)$  and residual bias  $\Delta b$  are reset.

In this way, the size of the original pretrained model after fine-tuning remains unchanged. Again, as in LORA, it is possible to reverse the training by subtracting the updates. Our proposal admits that after a given number  $N$  of training steps, say after each epoch, we merge weights and biases with (10) and (11); respectively. Thus, the formulas for the final updated weights and bias are given by

$$K_0 \leftarrow K_0 + \sum_{e=1}^E K_p^{(e)} \circledast K_d^{(e)} \quad (12)$$

and

$$b_0 \leftarrow b_0 + \sum_{e=1}^E \Delta b^{(e)}; \quad (13)$$

where  $K_d^{(e)}$  is the updated deepwise Kernel in the  $e$  training epoch; similarly for  $K_p^{(e)}$  and  $\Delta b^{(e)}$ . Last term in (12) updates the full kernel after the fine-tuning process. Now, by defining the vector  $w_k^{(e)}$  such that  $w_k^{(e)} = K_{p1k}^{(e)}$ . Thus, from (12):

$$\begin{aligned} |\Delta K_0 &= \sum_{e=1}^E K_p^{(e)} \circledast K_d^{(e)} \\ &= \begin{bmatrix} w_1^{(1)} K_d^{(1)} + w_1^{(2)} K_d^{(2)} + \dots + w_1^{(E)} K_d^{(E)} \\ w_2^{(1)} K_d^{(1)} + w_2^{(2)} K_d^{(2)} + \dots + w_2^{(E)} K_d^{(E)} \\ \vdots \\ w_C^{(1)} K_d^{(1)} + w_C^{(2)} K_d^{(2)} + \dots + w_C^{(E)} K_d^{(E)} \end{bmatrix} \\ &= \begin{bmatrix} \sum_e w_1^{(e)} K_d^{(e)} \\ \sum_e w_2^{(e)} K_d^{(e)} \\ \vdots \\ \sum_e w_C^{(e)} K_d^{(e)} \end{bmatrix}. \end{aligned} \quad (14)$$

The result is that the update kernel  $\Delta K_0$  is in the space that spans the individual kernels  $\mathbf{K}_s = [K_d^{(1)}, K_d^{(2)}, \dots, K_d^{(E)}]$ .

### 3.2 Generalization of CoLoRA to other dimensions

Separable convolutions in 3D are not implemented *Tensorflow* or *Pytorch* at the moment. Hence, here we present how to generalize the CoLoRA layer to other dimensions than two; *i.e.*, to one or three dimensions.

Since convolutions are linear operations, we can swap the order of the operation in (6) as

$$\Delta K = K_d \circledast K_p. \quad (15)$$

Figure 3 illustrates the new convolution order; compare with Fig. 2. This order of depth and point convolutions is used in the Inception Network [15]. The strategy is first to look for cross-channel correlations to reduce the dimension of the tensors along the channels. Next, the model looks for spatial correlations in a lower-dimension tensor (*i.e.*, with a single channel) [23]. To be consistent with the LoRA initialization, we initialize  $K_p$  with Glorot’s initializer ( $K_p \sim U$ ) [31] and  $K_d$  is set equal to zero.

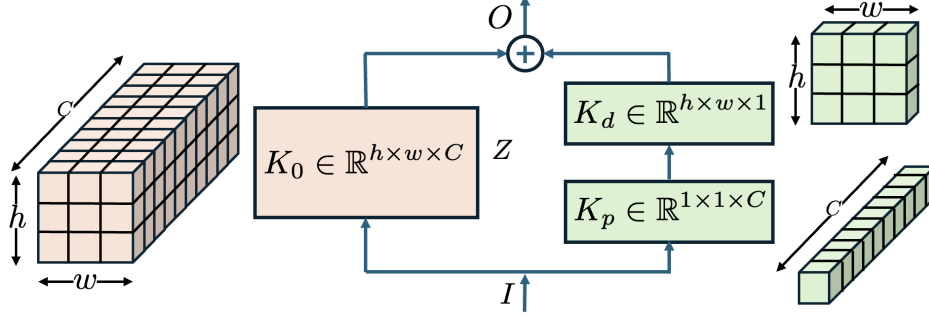


Figure 3: CoLoRA Layer using the inception operation order.

For the case convolutional 3D layer with input  $I \in \mathbb{R}^{H \times W \times D \times C}$ , each filter in the CoLoRA layer implements:

$$Z_1 = K_p \otimes I \quad (16)$$

$$Z_2 = K_d \otimes Z_1 \quad (17)$$

$$Z_3 = K_0 \otimes I \quad (18)$$

$$O = Z_3 + Z_2 \quad (19)$$

where  $\otimes$  denotes the correlation operation,  $K_p \in \mathbb{R}^{1 \times 1 \times 1 \times C}$  and  $K_d \in \mathbb{R}^{h \times w \times d \times 1}$ . Thus, if we apply the  $C'$  filters, it results in  $Z_1, Z_2, Z_3, O \in \mathbb{R}^{H \times W \times D \times C'}$ . This order of operations is computationally efficient: we computed  $C'$  weighted sums of the input tensor channels and computed  $C'$  2D-convolutions of a single channel. Moreover, it results in a straightforward generalization of the CoLoRA layers for fine-tuning convolutional layers in other dimensions than two, provided that we have a ready implementation of the Depthwise Convolution Layer.

Figure 4 illustrates the operations for the 2D convolution case. First, the input tensor  $I (H \times W \times C)$  is convolved with  $C'$  filters of  $1 \times 1 \times C$  (pixel-wise convolution); *i.e.*, we compute a weighted sum of the channels. Since each pixel-wise kernel produces a channel,  $Z_1$  preserves spatial dimensions but has  $C'$  channels. Now, each channel is independently convolved with a kernel  $K_d$  (with size equal to  $h \times w \times 1$ ). This result is denoted by  $Z_2$ .

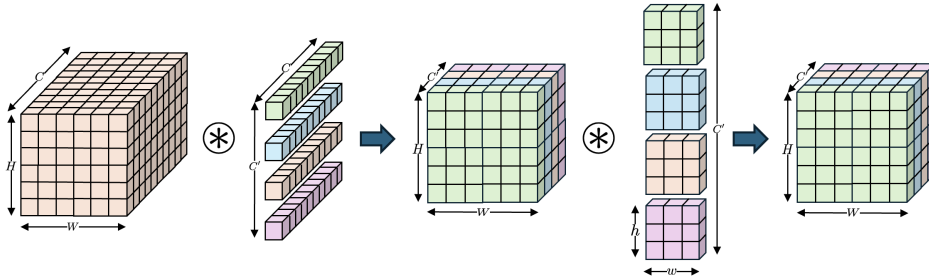


Figure 4: Illustration of the CoLoRA Layer internal operations.

### 3.3 Implementation Details

In our implementation, we selected as backbones two commonly used convolutional network architectures: VGG16 [12] and ResNet50v2 [13]; both pre-trained with ImageNet. VGG16 is widely used in knowledge transfer implementations due to the simplicity of the architecture. ResNet50v2 is selected for the parameter reduction compared to VGG16 while preserving high performance.

Due to its simplicity, we illustrate the case of the VGG16-CoLoRA model in Figure 5. We started by building a VGG16-based model with explicit Conv2D and activation “ReLU” layers. Then, we initialize the backbone weights with ImageNet-pretrained values. Afterward, we add a residual bypass to each Conv2D in the backbone. As we said, the residual bypass is a SeparatedConv2D layer with the same parameters (number of filters, stride, dilation, etc.) as the original Conv2D layer. We initially set the  $K_s$  kernel of the SeparatedConv2D layer according to [31]. On the other hand, we initialize the  $K_d$  kernel to zeros. To implement the problem-dependent decision stage, we first use a  $1 \times 1$  convolution that reduces the number of channels from 512 to 128. Then, we use two Fully Connected layers:



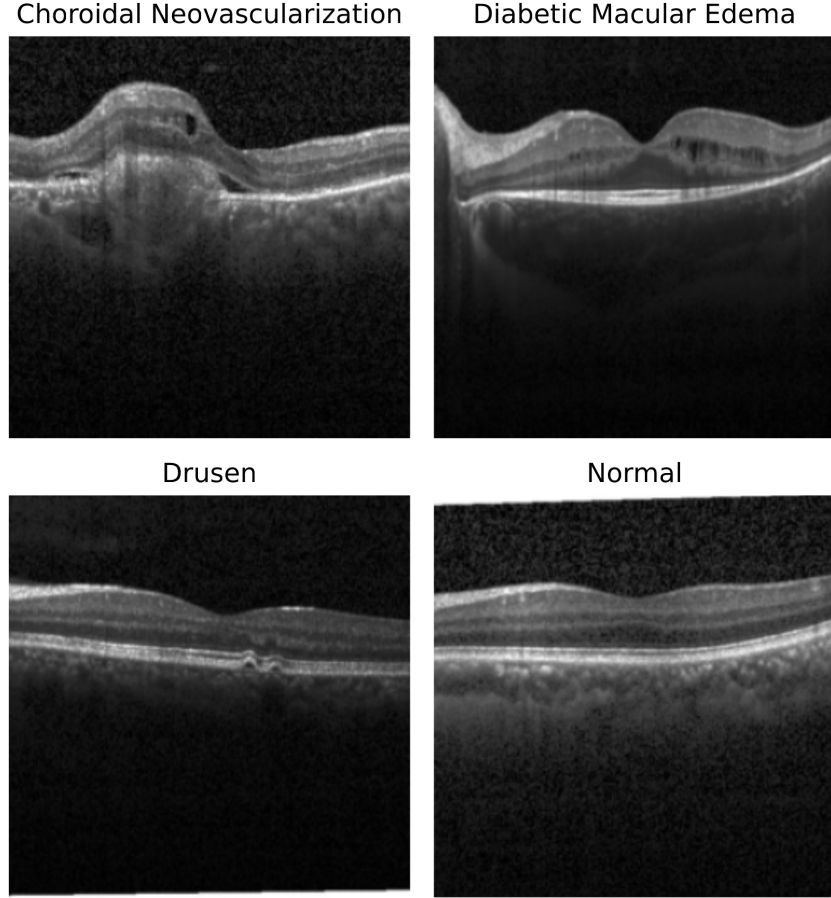


Figure 6: Example of the images in the OctMNISTv2 dataset.

contains the number of correctly classified images, and the off-diagonal elements contain the wrongly classified ones. Since our example is multiclass, we calculate the Recall (Sensitivity) using

$$R_i = \frac{C_{ii}}{[C \mathbf{1}]_i}; \quad (20)$$

where  $\mathbf{1}$  is a vector with all its entries equal to 1. Similarly, the Precision is calculated using

$$P_i = \frac{C_{ii}}{[\mathbf{1}^\top C]_i}. \quad (21)$$

Hence, the Total Accuracy is calculated with

$$ACC = \frac{\text{Tr}(C)}{\mathbf{1}^\top C \mathbf{1}}. \quad (22)$$

Finally, the Specificity is computed with

$$S_i = \frac{\text{Tr}(C) - C_i}{\mathbf{1}^\top C \mathbf{1} - [C \mathbf{1}]_i}. \quad (23)$$

Thus, the ROC curve is calculated as the ratio of  $P_i$  and  $(1 - S_i)$  when the detection threshold varies from 0 to 1.

### 4.3 VGG16-CoLoRA

We conducted ten independent fine-tunings of the VGG16–CoLoRA model for 20 epochs. After each epoch, we merge the Colora layer’s weights, reset the Depthwise convolution kernel and bias with zeros, and initialize the Pixelwise kernel weights. Also, at the end of each epoch, we evaluated the loss and accuracy (ratio of correctly classified data)

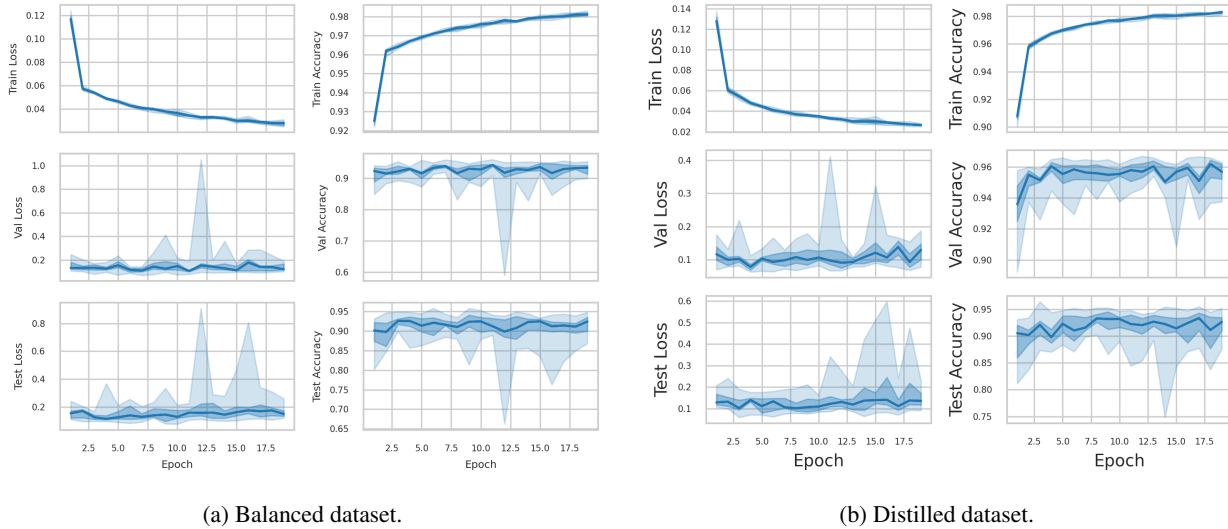


Figure 7: Historic curves of Loss and Accuracy for VGG16-CoLoRA model in bold line the median of 10 independent experiments, dark-blue region allocates 50% of the values (the IQR), and the light-blue region the total data.

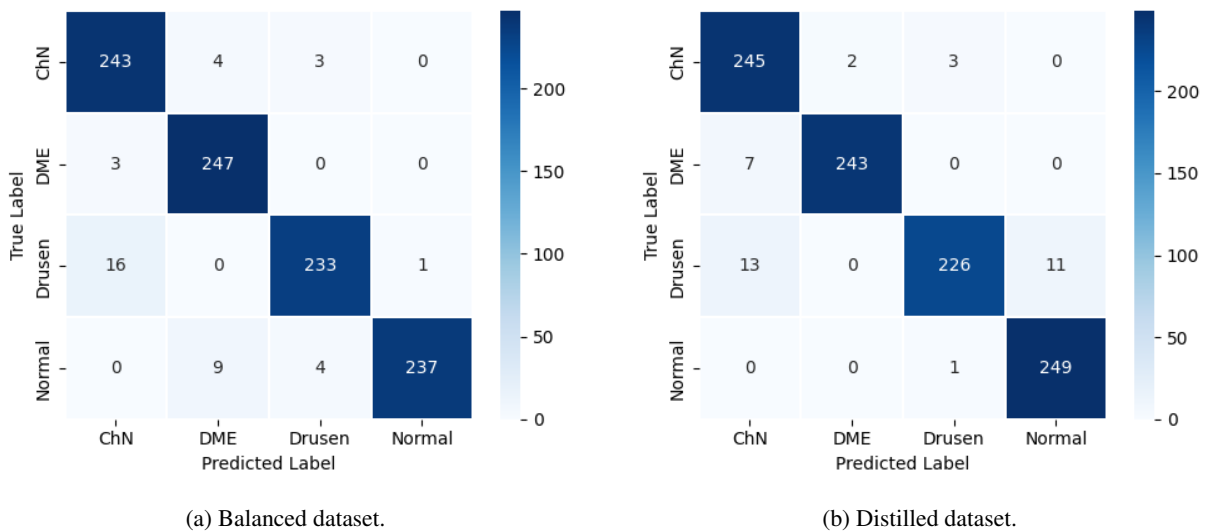


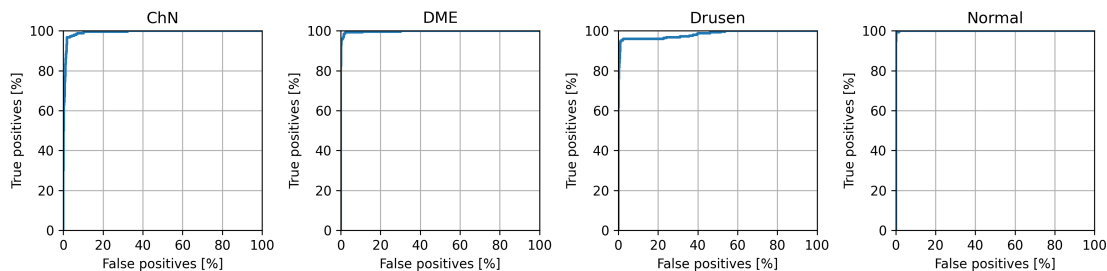
Figure 8: Confusion matrix of OctMNISTv2 test dataset for the VGG16-based classifier with CoLoRA strategy.

for the train, validation, and test datasets. Figure 7a shows the evolution of such metrics: the bold line corresponds to the median value per epoch, the dark blue region allocates 50% of the values closer to the median (the interquartile range, IQR), and the light blue shows the full interval of the values. The loss and accuracy (ratio of correctly classified data) are smooth and consistent (similar to the experiments): the loss decreases, and the accuracy approaches one. This characterizes a correct parameter update by CoLoRA-based fine-tuning, the main contribution of this work. In addition, we observe that the median and IQR accuracy for the validation and test data sets remain relatively stable with a slight growth trend. The 75% best results can be marked as a success. We note that the small number of images in the test data set results in a larger variance of the metrics compared to the validation data set. Thus, we select the model with the best accuracy in the test dataset to report metrics. The performance of fine-tuning the parameters of the VGG16-based model with the CoLoRA strategy is reported in the confusion matrix in Fig. 8a. Table 2 presents the AUC-ROC and accuracy metrics. Then, Fig. 9a shows the ROC curves.

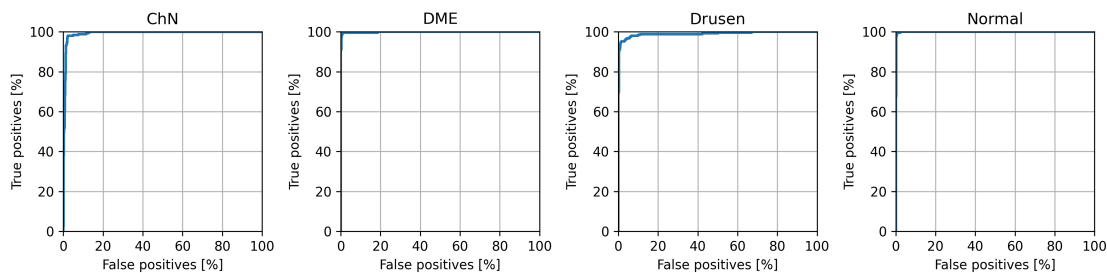
As mentioned, previously reported experiments are based on a balanced database using the first 7754 data points from each class (the number of cases in the smallest class). To perform a more appropriate selection, we employ a data distillation strategy. Therefore, we sort the training data by prediction entropy with the best pre-trained model.

| Class  | AUC ROC | Recall | Precision |
|--------|---------|--------|-----------|
| ChN    | 0.992   | 0.972  | 0.927     |
| DME    | 0.998   | 0.988  | 0.950     |
| Drusen | 0.983   | 0.932  | 0.971     |
| Normal | 0.999   | 0.949  | 0.996     |
| Avg.   | 0.993   | 0.9600 | 0.961     |

Table 2: Performance metrics of the VGG16-CoLoRA model trained on the BALANCED dataset.



(a) Balanced dataset.



(b) Distilled dataset.

Figure 9: ROC curves for the VGG16-based classifier trained with CoLoRA on the OctMNISTv2

Accordingly, we discard the 10 data points with the highest entropy and keep the next 7040 data points for each class. Figure 10 shows the entropy of the distilled data points. Fig. 11a shows the first 25 data points with the highest entropy of each class; the first 10 data points were discarded in the distillation process. Fig. 12a shows the corresponding predictions. In constant, Fig. 11b shows 25 data points per class with low prediction entropy (elements 5000 to 5025 in the sorted list) and Fig. 12b with the corresponding predictions.

| Class  | Transfer |       |       | CoLoRA |       |       |
|--------|----------|-------|-------|--------|-------|-------|
|        | AUC      | Rec.  | Prec. | AUC    | Rec.  | Prec. |
| ChN    | 0.980    | 0.960 | 0.863 | 0.992  | 0.980 | 0.924 |
| DME    | 0.983    | 0.932 | 0.955 | 0.999  | 0.972 | 0.992 |
| Drusen | 0.975    | 0.824 | 0.915 | 0.990  | 0.904 | 0.983 |
| Normal | 0.993    | 0.948 | 0.937 | 0.998  | 0.996 | 0.958 |
| Avg.   | 0.983    | 0.916 | 0.918 | 0.995  | 0.963 | 0.964 |

Table 3: Performance metrics of the VGG16-CoLoRA model on the DISTILLED dataset.

The final training is performed on the distilled data. We perform the refinement using CoLoRA 10 times for 20 epochs and select the best-performing model in any epoch. The loss and accuracy curves are shown in Fig. 7b, the confusion matrix in Fig. 8b and the ROC curves in 9b. Finally, Table 3 presents the performance metrics of VGG16-CoLoRA for each class in the dataset. Table 4 compares the performance of this versus other reference and state-of-the-art models: MedViT (v1 [16] and v2 [17]), MedKAN [19], and MedMamba [18]. These models require full training, which makes them computationally expensive as the number of parameters increases. However, although the simple model based on pretrained VGG16 and fine-tuned with CoLoRA has 15.6 million trainable parameters, only 2.5 million are updated using backpropagation; the rest are updated by parameter merging after each epoch. As we can see, VGG16-CoLoRA improves the accuracy of MedViT-Large by more than 1% and surpasses the performance of more complex models

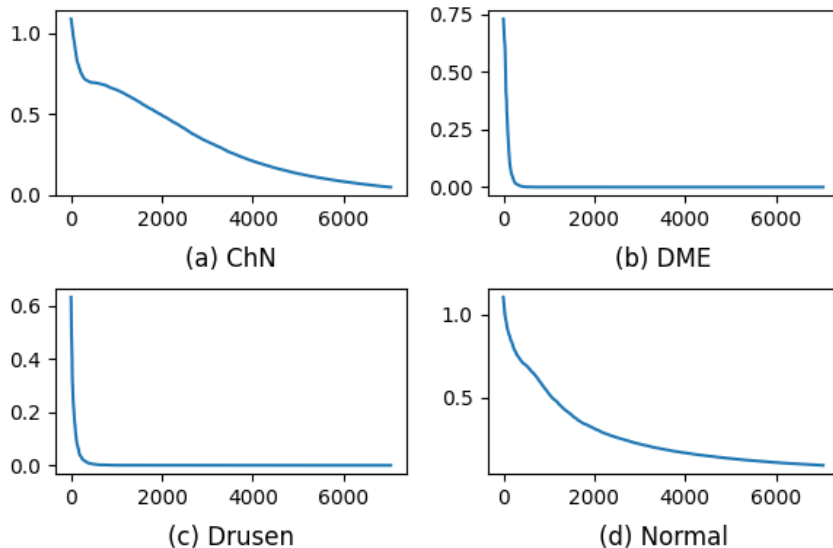


Figure 10: Sorted entropy of selected (distilled) 7040 data for each class.

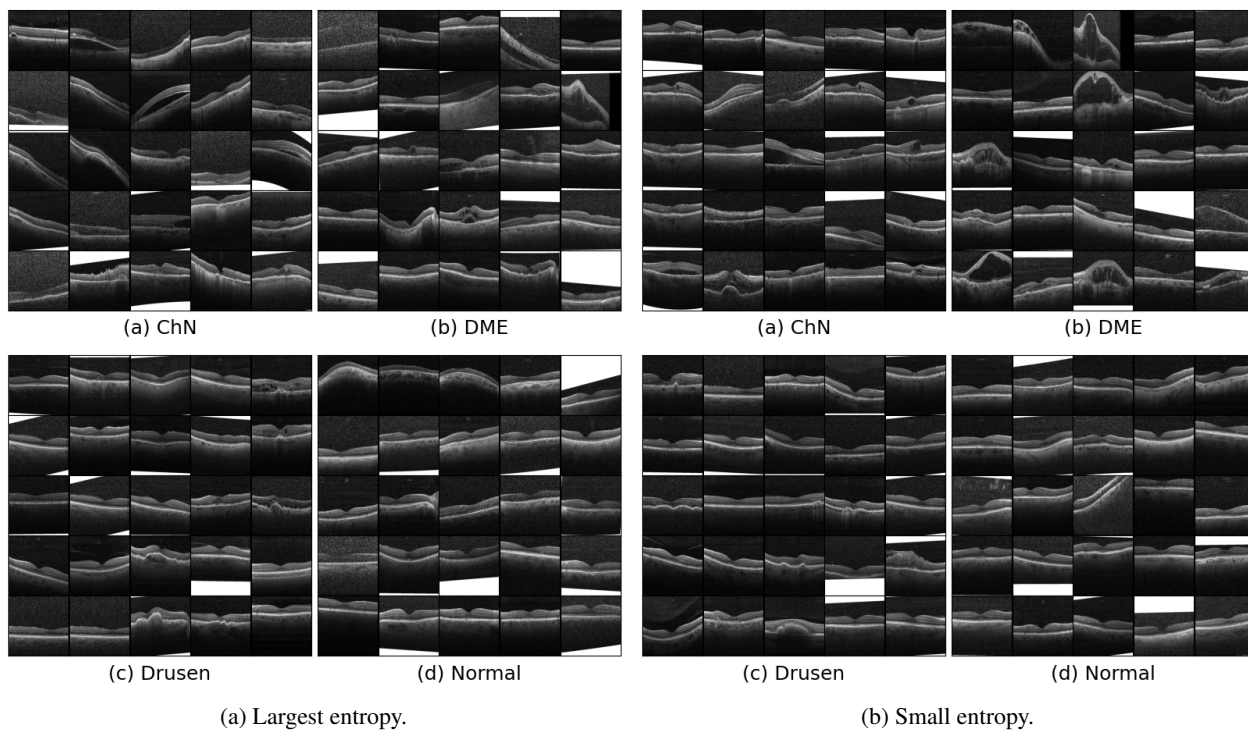


Figure 11: Example images in the balanced dataset grouped by entropy.

based on Vision Transformers [16, 17], Kolmogorov-Arnold networks [19], and state-space models combined with a discretization process [18].

#### 4.4 ResNet50-CoLoRA

We expanded our evaluation to include the ResNet50 model under the same experimental conditions as the VGG16. After each epoch, we merged the CoLoRA layer weights, reset the depthwise convolution kernel and bias to zero, and

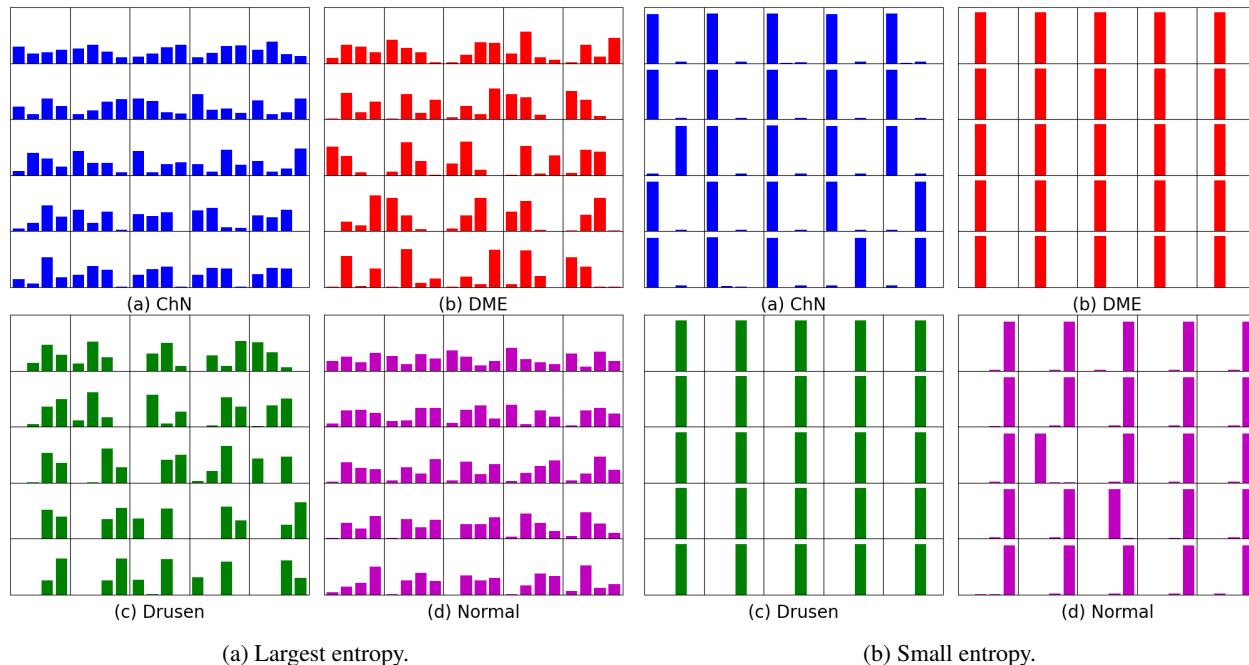


Figure 12: Predictions on the example images in the balanced dataset.

| Method                   | AUC          | Acc.         | Params.            |
|--------------------------|--------------|--------------|--------------------|
| Resnet-18 (28) [32]      | 0.951        | 0.758        |                    |
| ResNet-50 (224) [32]     | 0.951        | 0.750        |                    |
| Dedicated CNN (28) [35]  |              | 0.760        |                    |
| ResNet-50 (224) [35]     |              | 0.776        |                    |
| MedViTv1-T [16]          | 0.961        | 0.767        | 15.2M              |
| MedViTv1-S [16]          | 0.960        | 0.782        |                    |
| MedViTv1-L [16]          | 0.945        | 0.761        |                    |
| MedKAN-S [19]            | 0.993        | 0.921        | 11.5M              |
| MedKAN-B [19]            | <b>0.996</b> | 0.927        | 24.6M              |
| MedKAN-L [19]            | 0.994        | 0.925        | 48.0M              |
| MedMamba-T [18]          | 0.992        | 0.918        | 15.2M              |
| MedMamba-S [18]          | 0.991        | 0.929        | 23.5M              |
| MedMamba-B [18]          | <b>0.996</b> | 0.927        | 48.1M              |
| MedMamba-X [18]          | 0.993        | 0.928        |                    |
| MedViTv2-T [17]          | 0.993        | 0.927        |                    |
| MedViTv2-S [17]          | 0.994        | 0.942        |                    |
| MedViTv2-B [17]          | <b>0.996</b> | 0.944        | 32.3M              |
| MedViTv2-L [17]          | <b>0.996</b> | 0.952        |                    |
| ResNet50-Trans. Learning | 0.983        | 0.903        | 37.7M              |
| ResNet50-CoLoRA          | 0.992        | 0.951        | 14.2M <sup>†</sup> |
| VGG16-Trans. Learning    | 0.982        | 0.916        | 0.9M               |
| VGG16-CoLoRA             | 0.995        | <b>0.963</b> | 2.6M <sup>‡</sup>  |

Table 4: Performance comparison of a based model fine-tuned with CoLoRA (proposal) with SoTA methods in the OCTMNIST image classification task. <sup>†</sup> 14.7M are trained by backpropagation of 37.7M total. <sup>‡</sup> 2.5M are trained by backpropagation of 15.6M.

initialized the pixelwise kernel weights. At the end of each epoch, we assessed the loss and accuracy of the training, validation, and test images, using only the OCTMNIST balanced dataset.

Initially, as a baseline, we froze a ResNet50 model with pre-trained backbone and only trained the classification head. However, this configuration resulted in poor performance, producing accuracy values significantly lower than the baseline reported in [32]. This confirmed that minimal adaptation is insufficient for this architecture in our domain-specific task. Subsequently, we performed a full fine-tuning of the ResNet50 model, allowing all layers to receive gradient updates. This approach increased the test accuracy to 0.903; however, it introduced significant computational overhead due to the model’s size of more than 37 million trainable parameters, resulting in slow convergence during training. To address such limitations, we implemented our proposed CoLoRA-based fine-tuning strategy while keeping the ImageNet-pretrained backbone frozen. We selectively added and updated CoLoRA layers. This configuration achieved a test accuracy of 0.951, representing a substantial improvement in efficiency and performance over previous configurations. We also tested this approach using the distilled version and the complete dataset. Although the ResNet50-CoLoRA model outperformed several state-of-the-art methods, it did not surpass the best accuracy achieved with the VGG16-CoLoRA model. Therefore, our future work will involve a deeper investigation of convolutional neural network architectures equipped with CoLoRA layers. Our goal is to identify optimal configurations and further clarify the generalizability and limitations of this fine-tuning strategy across different convolutional models.

## 5 Conclusions

We have presented CoLoRA, a novel extension of Low-Rank Adaptation (LoRA) to convolutional neural networks, which decomposes convolutional kernel updates into lightweight depth-wise and point-wise components. This design reduces the number of trainable parameters by more than 80% compared to traditional fine-tuning, while preserving the original model size and enabling efficient parameter merging after each epoch.

In a comprehensive case study on the OCTMNIST dataset for the classification of retinal diseases, our VGG16-CoLoRA and ResNet50-CoLoRA models achieved state-of-the-art performance, with accuracy improvements of approximately 1% and AUC gains of up to 0.013 over strong baselines of Vision Transformer, state space and Kolmogorov-Arnold. In addition, training times per epoch were reduced by nearly 20% relative to the simple transfer learning strategy, demonstrating CoLoRA’s practical efficiency for medical imaging tasks.

Although this work focuses on 2D image classification, the CoLoRA paradigm naturally extends to 1D and 3D convolutions; future implementations will explore volumetric data and semantic segmentation in medical volumes. Investigating adaptive rank selection strategies and dynamic merging schedules could further optimize the parameter–performance trade-off. Finally, integrating CoLoRA with complementary EPFT techniques (e.g., prompt tuning or adapter fusion) may unlock additional gains in multimodal and multitask settings.

In general, CoLoRA provides a flexible, parameter-efficient fine-tuning framework for convolutional architectures, offering significant advantages in both computational cost and accuracy for real-world medical imaging applications.

**Acknowledges.** Work supported in part by SECIHTI, Mexico (Grant CB-A1-43858).

## References

- [1] C. Zhou, Q. Li, C. Li, J. Yu, Y. Liu, G. Wang, K. Zhang, C. Ji, Q. Yan, L. He, et al., A comprehensive survey on pretrained foundation models: A history from BERT to ChatGPT, *International Journal of Machine Learning and Cybernetics* (2024) 1–65.
- [2] D. Myers, R. Mohawesh, V. I. Chellaboina, A. L. Sathvik, P. Venkatesh, Y.-H. Ho, H. Henshaw, M. Alhawawreh, D. Berdik, Y. Jararweh, Foundation and large language models: fundamentals, challenges, opportunities, and social impacts, *Cluster Computing* 27 (2024) 1–26.
- [3] H. Naveed, A. U. Khan, S. Qiu, M. Saqib, S. Anwar, M. Usman, N. Akhtar, N. Barnes, A. Mian, A comprehensive overview of large language models, *arXiv preprint arXiv:2307.06435* (2023).
- [4] Z. Han, C. Gao, J. Liu, J. Zhang, S. Q. Zhang, Parameter-efficient fine-tuning for large models: A comprehensive survey, *Transactions on Machine Learning Research* (2024).
- [5] N. Houlsby, A. Giurgiu, S. Jastrzebski, B. Morrone, Q. De Laroussilhe, A. Gesmundo, M. Attariyan, S. Gelly, Parameter-efficient transfer learning for NLP, in: K. Chaudhuri, R. Salakhutdinov (Eds.), *Proceedings of the 36th International Conference on Machine Learning*, volume 97 of *Proceedings of Machine Learning Research*, PMLR, 2019, pp. 2790–2799.
- [6] J. Pfeiffer, A. Kamath, A. Rücklé, K. Cho, I. Gurevych, Adapterfusion: Non-destructive task composition for transfer learning, in: *Proceedings of the 16th Conference of the European Chapter of the Association for Computational Linguistics: Main Volume*, 2021, pp. 487–503.

- [7] A. Kirillov, E. Mintun, N. Ravi, H. Mao, C. Rolland, L. Gustafson, T. Xiao, S. Whitehead, A. C. Berg, W.-Y. Lo, P. Dollár, R. Girshick, Segment anything, in: Proceedings of the IEEE/CVF International Conference on Computer Vision (ICCV), 2023, pp. 4015–4026.
- [8] J. Wu, Z. Wang, M. Hong, W. Ji, H. Fu, Y. Xu, M. Xu, Y. Jin, Medical SAM adapter: Adapting segment anything model for medical image segmentation, *Medical Image Analysis* (2025) 103547. doi:<https://doi.org/10.1016/j.media.2025.103547>.
- [9] R. Dutt, L. Ericsson, P. Sanchez, S. A. Tsiftaris, T. Hospedales, Parameter-efficient fine-tuning for medical image analysis: The missed opportunity, in: *Medical Imaging with Deep Learning*, 2024.
- [10] H. E. Kim, A. Cosa-Linan, N. Santhanam, M. Jannesari, M. E. Maros, T. Ganslandt, Transfer learning for medical image classification: A literature review, *BMC medical imaging* 22 (2022) 69.
- [11] A. W. Salehi, S. Khan, G. Gupta, B. I. Alabdullah, A. Almjally, H. Alsolai, T. Siddiqui, A. Mellit, A study of CNN and transfer learning in medical imaging: Advantages, challenges, future scope, *Sustainability* 15 (2023) 5930.
- [12] K. Simonyan, Very deep convolutional networks for large-scale image recognition, arXiv preprint arXiv:1409.1556 (2014).
- [13] K. He, X. Zhang, S. Ren, J. Sun, Deep residual learning for image recognition, in: Proceedings of the IEEE Conference on Computer Vision and Pattern Recognition (CVPR), 2016, pp. 770–778.
- [14] K. He, X. Zhang, S. Ren, J. Sun, Identity mappings in deep residual networks, in: *Computer Vision–ECCV 2016: 14th European Conference, Amsterdam, The Netherlands, October 11–14, 2016, Proceedings, Part IV 14*, Springer, 2016, pp. 630–645.
- [15] C. Szegedy, W. Liu, Y. Jia, P. Sermanet, S. Reed, D. Anguelov, D. Erhan, V. Vanhoucke, A. Rabinovich, Going deeper with convolutions, in: Proceedings of the IEEE Conference on Computer Vision and Pattern Recognition (CVPR), 2015.
- [16] O. N. Manzari, H. Ahmadabadi, H. Kashiani, S. B. Shokouhi, A. Ayatollahi, MedViT: A robust vision transformer for generalized medical image classification, *Computers in Biology and Medicine* 157 (2023) 106791.
- [17] O. N. Manzari, H. Asgariandehkordi, T. Koleilat, Y. Xiao, H. Rivaz, Medical image classification with KAN-integrated transformers and dilated neighborhood attention, arXiv preprint arXiv:2502.13693 (2025).
- [18] Y. Yue, Z. Li, Medmamba: Vision mamba for medical image classification, arXiv preprint arXiv:2403.03849 (2024).
- [19] Z. Yang, J. Zhang, X. Luo, Z. Lu, L. Shen, MedKAN: An advanced Kolmogorov-Arnold network for medical image classification, arXiv preprint arXiv:2502.18416 (2025).
- [20] E. J. Hu, Y. Shen, P. Wallis, Z. Allen-Zhu, Y. Li, S. Wang, L. Wang, W. Chen, LoRA: Low-rank adaptation of large language models, in: *International Conference on Learning Representations*, 2022.
- [21] M. Awais, M. Naseer, S. Khan, R. M. Anwer, H. Cholakkal, M. Shah, M.-H. Yang, F. S. Khan, Foundation models defining a new era in vision: A survey and outlook, *IEEE Transactions on Pattern Analysis and Machine Intelligence* 47 (2025) 2245–2264. doi:10.1109/TPAMI.2024.3506283.
- [22] R. Venkatesan, B. Li, *Convolutional neural networks in visual computing: A concise guide*, CRC Press, 2017.
- [23] F. Chollet, Xception: Deep learning with depthwise separable convolutions, in: Proceedings of the IEEE Conference on Computer Vision and Pattern Recognition (CVPR), 2017.
- [24] A. G. Howard, M. Zhu, B. Chen, D. Kalenichenko, W. Wang, T. Weyand, M. Andreetto, H. Adam, MobileNets: Efficient convolutional neural networks for mobile vision applications (2017), arXiv preprint arXiv:1704.04861 126 (2017).
- [25] J. He, C. Zhou, X. Ma, T. Berg-Kirkpatrick, G. Neubig, Towards a unified view of parameter-efficient transfer learning, in: *International Conference on Learning Representations*, 2022.
- [26] J.-M. O. Steitz, S. Roth, Adapters strike back, in: Proceedings of the IEEE/CVF Conference on Computer Vision and Pattern Recognition, 2024, pp. 23449–23459.
- [27] S.-A. Rebuffi, H. Bilen, A. Vedaldi, Learning multiple visual domains with residual adapters, *Advances in neural information processing systems* 30 (2017).
- [28] S.-A. Rebuffi, H. Bilen, A. Vedaldi, Efficient parametrization of multi-domain deep neural networks, in: Proceedings of the IEEE conference on computer vision and pattern recognition, 2018, pp. 8119–8127.

- [29] Z.-C. Chen, Y.-S. Sung, H.-y. Lee, Chapter: Exploiting convolutional neural network adapters for self-supervised speech models, in: 2023 IEEE International Conference on Acoustics, Speech, and Signal Processing Workshops (ICASSPW), IEEE, 2023, pp. 1–5.
- [30] N. Houlsby, A. Giurgiu, S. Jastrzebski, B. Morrone, Q. De Laroussilhe, A. Gesmundo, M. Attariyan, S. Gelly, Parameter-efficient transfer learning for NLP, in: International conference on machine learning, PMLR, 2019, pp. 2790–2799.
- [31] X. Glorot, Y. Bengio, Understanding the difficulty of training deep feedforward neural networks, in: Proceedings of the thirteenth international conference on artificial intelligence and statistics, JMLR Workshop and Conference Proceedings, 2010, pp. 249–256.
- [32] J. Yang, R. Shi, B. Ni, MedMNIST classification decathlon: A lightweight AutoML benchmark for medical image analysis, in: IEEE 18th International Symposium on Biomedical Imaging (ISBI), 2021, pp. 191–195.
- [33] J. Yang, R. Shi, D. Wei, Z. Liu, L. Zhao, B. Ke, H. Pfister, B. Ni, MedMNIST v2-a large-scale lightweight benchmark for 2D and 3D biomedical image classification, *Scientific Data* 10 (2023) 41.
- [34] N. Ferrara, Vascular endothelial growth factor and age-related macular degeneration: From basic science to therapy, *Nature Medicine* 16 (2010) 1107–1111.
- [35] M. Wilhelmi, A. Rusiecki, Simple CNN as an alternative for large pretrained models for medical image classification-MedMNIST case study, *Procedia Computer Science* 239 (2024) 1298–1303.